Rheol Acta (2014) 53:133–141
DOI 10.1007/s00397-013-0746-y

ORIGINAL CONTRIBUTION

The rheology of suspensions of porous zeolite particles in polymer solutions

Kayode O. Olanrewaju · Tae-Hyun Bae · Sankar Nair · Victor Breedveld

Received: 15 April 2013 / Revised: 5 October 2013 / Accepted: 19 November 2013 / Published online: 15 December 2013

Abstract We present data and predictive models for the shear rheology of suspended zeolite particles in polymer solutions. It was found experimentally that suspensions of zeolite particles in polymer solutions have relative viscosities that dramatically exceed the Krieger–Dougherty predictions for hard sphere suspensions. Our investigations show that the major origin of this discrepancy is due to the selective absorption of solvent molecules from the suspending polymer solution into zeolite pores. The effect raises both the polymer concentration in the suspending medium and the particle volume fraction in the suspension. Consequently, both the viscosity of the polymer solution and the particle contribution to the suspension viscosity are increased. We propose a predictive model for the viscosity of porous zeolite suspensions by incorporating a solvent absorption parameter, α, into the Krieger–Dougherty model. We experimentally determined the solvent absorption parameter by comparing viscosity data for suspensions of porous and nonporous MFI zeolite particles. Our results are in good agreement with the theoretical pore volume of MFI particles.

Keywords Viscosity · Shear rheology · Suspension · Absorption parameter · MFI zeolite · Zeolite particles

K. O. Olanrewaju (✉) · T.-H. Bae · S. Nair · V. Breedveld
School of Chemical and Biomolecular Engineering,
Georgia Institute of Technology, 311 Ferst Drive,
Atlanta, GA 30332-0100, USA
e-mail: kolanrewaj3@gatech.edu

Introduction

Industrial-scale gas separations by means of polymeric membranes have attracted a lot of attention in recent years. However, the performance of such membranes seems to be limited by a general trade-off between selectivity and permeability, often referred to as the Robeson upper bound (Robeson 1991, 2008). The desire for better gas separation efficiencies has led to the development of mixed matrix membranes (MMMs) (Chung et al. 2007; Mahajan and Koros 2000, 2002a, b; Moore et al. 2004; Paul and Kemp 1973) which combine the processability of polymer solutions with the high selectivity of zeolite particles. For gas membranes, hollow fiber modules are preferred due to their high surface area per unit volume for separation. The membrane dope for the selective layer of dual-layer MMMs consists of zeolite particles dispersed in a polymer solution, while the support layer is made from a polymer solution. The spinning of membrane dopes into hollow fibers of desired dimensions requires a good measure and understanding on the rheology of the membrane dope formulations (Ekiner and Vassilatos 1990, 2001; Wallace et al. 2006). To our knowledge, there is no report in the literature were the rheology of porous zeolite particles in polymer solutions has been addressed. This study addresses some of the unique ramifications of the presence of porous zeolite particles on the rheology of polymer solutions.

The rheology of model hard sphere suspensions has long been a subject of theoretical and experimental investigations. Fundamental and empirical models exist that predict the viscosity of hard sphere suspensions from low to high particle loadings (Batchelor 1977; Einstein 1906, 1911; Krieger and Dougherty 1959). However, most zeolite

particles are not spherical. Particle nonsphericity (Jeffery 1922a, b; Mueller et al. 2010; Stimson and Jeffery 1926) invariably results in additional viscous dissipations not accounted for by hard sphere models. For nonspherical particles with simple prolate or oblate axial symmetry, extensions of hard sphere models can still be used, using the particle aspect ratio as an additional parameter (Mueller et al. 2010). The aspect ratio (1 for spheres, >1 for nonspherical particles) affects the value of two key parameters: the intrinsic viscosity and the maximum packing volume fraction (Jeffery 1922a; Kitano et al. 1981; Mueller et al. 2010; Pabst et al. 2006). In general, as the aspect ratio of particles increases, the intrinsic viscosity increases, and the maximum packing fraction decreases,both effects act to enhance the viscosity of a suspension. For hard sphere suspensions, the size of suspended particles itself has no effect on rheology; the volume fraction is the only relevant parameter. The aspect ratio of MFI particles, however, depends on particle size due to unequal growth rates in different planes during crystal formation (Flanigen et al. 1978; Fyfe et al. 1982). Based on this peculiar feature of MFI particles, one would expect the viscosity of suspensions of MFI particles to show size dependency. In addition, zeolite particles may possess surface silanol groups or other functional groups that may dissociate, causing them to acquire surface charge in aqueous solutions. Suspensions of charged particles have enhanced viscosities due to electroviscous effects (Booth 1950; Russel 1976; Vaynberg and Wagner 2001; Watterson and White 1981; Zurita et al. 1994). In addition to the deviations resulting from particle peculiarities, the rheology of suspensions in elastic matrices is also impacted by the nature of the suspending medium. Particularly at high shear rates where the viscosity becomes nonlinear, shear-induced relaxation spectrum rearrangements could lead to the formation of anisotropic structures and changes in macromolecular entanglements. These macromolecular transformations may induce nonlinearity in the suspensions such as migration, alignment, and flocculation as reported in the literature (Malkin 2012; Zhou et al. 1999; de Oliveira et al. 2011; Pasquino et al. 2012). Furthermore, in the linear flow regime, the elasticity of the suspension medium could impact the viscosity of overall suspension as previously reported (Pasquino et al. 2008; Snijkers et al. 2013). This paper investigates the deviations from model suspensions behavior arising from the porous structure of zeolite particles.

Specifically, in this paper, we report on data and semiempirical models for the viscosity of suspensions of MFI zeolite particles in polymer solutions. As will be shown, the viscosity of zeolite suspensions may not be readily predicted by hard sphere models. Zeolite particles often have internal pores that are sufficiently large to be accessible to water and other small solvent molecules, while excluding the larger macromolecules. The selective absorption of solvent molecules from the suspending medium results in concentration changes of both polymers in the suspending phase and particles in the overall suspension, which can lead to dramatic increases in the viscosity of such suspensions. To correctly predict the viscosity of zeolite suspensions in polymer solutions, the quantity of absorbed solvent must first be determined. This can then be used to calculate the effective particle volume fraction and effective polymer concentration. It should be noted that for the specific case described in this paper (MFI zeolite particles with NMP), the molecular mechanism for solvent extraction from the medium is adsorption onto the zeolite pore walls. However, the phenomenon described here, viscosity enhancement due to solvent loss from the suspending polymer solution into porous particles, is independent of the molecular mechanism; hence, we prefer to use the term absorption instead of adsorption.

We describe the effect of solvent absorption on the viscosity of zeolite particles in polymer solutions in the form of a new mathematical model. To this end, a solvent absorption parameter, α, was defined, and experiments were designed to quantify it. The experimental determination of α is based on a direct comparison of the viscosities of porous (calcined) and nonporous (uncalcined) MFI zeolite suspensions in polymeric solutions of polyetherimide (Ultem®) in *N*-methyl pyrrolidinone (NMP). This system was chosen because of its relevance for MMM hollow fiber spinning, but the concepts developed in this paper are more broadly applicable.

Experimental

Materials The polymer used in all experiments reported in this study is polyetherimide (Ultem 1000, MW ~ 61,000) purchased from GE Plastics. The solvent of choice is NMP (purity 99.95 %), purchased from Sigma-Aldrich and used as received.

Pure silica MFI particles of 130 nm (shown in Fig. 1) were used in this study. Pure silica MFI crystals were hydrothermally synthesized using tetraethylorthosilicate (TEOS, Sigma-Aldrich) and tetrapropylammonium hydroxide (TPAOH, 40 % in water, Alfa Aesar) as silica source and structure-directing agent, respectively. The synthesis is described in more detail in references Cheng et al. (2008) and Schoeman (1997a, b). In order to promote good dispersion of the particles in the polymer solutions, we used silane-treated MFI (ST MFI) and Ultem-sized MFI (USZ-MFI) instead of untreated pure silica MFI for our membrane dope preparation. The method of surface functionalization is available in greater detail in the paper by Husain and Koros (2007).

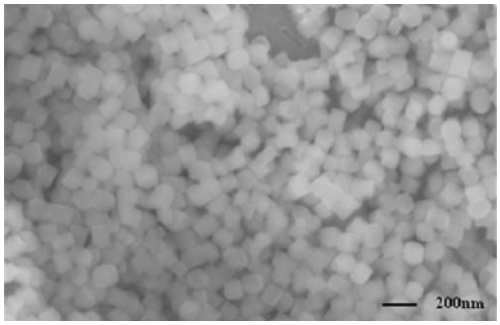

Fig. 1 SEM micrograph of pure silica MFI zeolite particles

Immediately after synthesis, MFI particles are uncalcined and nonporous with a density of 1.99 g cm^{-3} (Flanigen et al. 1978). The microporous form is obtained by calcination in air at 500–600 °C for 8 h. Calcination is the thermal decomposition of the organic templates to yield the calcined (porous) MFI of a lower density (Flanigen et al. 1978). Indeed, pure silica MFI is a highly robust inorganic crystal which is stable up to 700∼800 °C. The calcination process only removes the structure-directing agent, and the morphology and crystal structure of MFI is always retained. Therefore, the size and morphology of pure silica MFI crystals should be the same before and after the calcination as long as the zeolites are produced from the same batch, indicating that the effect of particle size variation caused by the calcination on the membrane dope solution rheology can be ruled out. Meanwhile, the average size of MFI crystals in SEM image was about 131 nm with 6 nm of standard deviation, as analyzed by ImageJ, a freely available software. Particle size distribution (PSD) affects rheology at high particle loadings (Metzner 1985). The effect of PSD on suspension viscosity is negligible in the present case since the PSD is narrow, and particle loading is much less than the maximum packing fraction.

Sample preparation The polymer was dried at 120 °C for 6 h before use, while the NMP solvent was used without any pretreatment. Polymer solutions were prepared by adding calculated amounts of dried Ultem polymer to NMP and allowing the polymer to fully dissolve on a slow roller for at least 72 h at room temperature before measurements were performed. The suspensions were prepared carefully, following a well-defined protocol to facilitate good dispersion of the particles in a 30 wt% Ultem/NMP solution. First, the required mass of zeolite was weighed on an analytical balance, and some solvent was added, followed by horn sonication (Biologics Inc., Manassas, VA) three to five times in 30-s bursts and with at least 1-min rest intervals between successive steps. The sonication step was used to break apart agglomerates of fired particles. The next step was a "priming" step in which a small quantity of preprepared polymer solution is added to the sonicated suspension, and the mixture is subsequently allowed to mix for 10–30 min on a slow roller. This step aims to sterically stabilize the suspension against particle aggregation through polymer adsorption. Finally, the remaining amount of polymer is added to the mixture as dried powder to bring the final concentration of all components to the desired dope composition. The suspension is placed on a slow roller until the polymer is completely dissolved for at least 24 h. Subsequently, the suspension is confirmed to be well dispersed by optical microscopy.

Density measurements The density of calcined MFI particles, ρ_{cal}, was determined by measuring the weight of a fixed volume of MFI before and after calcination, m_{uncal} and m_{cal}, respectively. Using the assumption that the external physical volume occupied by uncalcined and calcined MFI is the same, the density of calcined MFI was calculated to be 1.76 g cm^{-3} from the following equation:

$$\rho_{cal} = \frac{m_{cal}}{m_{uncal}} \rho_{uncal} \quad (1)$$

The density of polymer solutions was determined with a pycnometer by measuring the weight of known sample volumes. The variation of the density of Ultem/NMP solutions as a function of polymer weight fraction is presented in Fig. 2. This information is important for the analysis of suspensions in which the polymer concentration in the suspending medium varies.

Rheological measurements The shear viscosity of the pure polymer solutions was measured over a range of shear rates (0.1–100 s^{-1}) at 50 °C with a stress-controlled rheometer (MCR 300, Anton Paar) and Couette geometry (CC10; cup inside diameter 10.845 mm and bob outer diameter 10.000 mm). The viscosities reported for the polymer solutions and zeolite suspensions in this paper were measured at low shear rates, before the onset of shear thinning, and represent the zero shear viscosity. The specific viscosity is plotted as a function of Ultem/NMP solution concentration in Fig. 3a. Figure 3a shows the overlap concentration

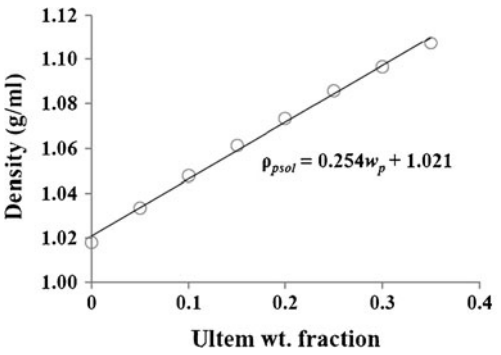

Fig. 2 Density of Ultem/NMP solutions at 50 °C as a function of polymer concentration

at 0.02 g/ml and the critical entanglement concentration at 0.1 g/ml. The power law fit for the data in the second concentration regime has a power 2 scaling implying a theta solvent. The regime covering concentrations beyond the critical entanglement concentration, 0.1 g/ml, is the relevant regime since the zeolite particles are suspended in a 30 wt% Ultem/NMP solution. Thus, the viscosity of solutions are plotted and fitted for concentrations ranging from 0.1 to 0.35 wt% as shown in Fig. 3b. The exponential fit of viscosity with respect to concentration was chosen because it minimizes the fitting error. Flow curve measurements were also performed at different MFI particle loadings in the suspending media with a nominal concentration of 30 wt% Ultem/NMP for both uncalcined and calcined MFI particles. The fixed polymer concentration used for these zeolite suspensions represents an optimized dope composition that enables good hollow fiber spinning properties for Ultem/NMP solutions as reported by Husain (2006).

Theory

As previously discussed, calcined MFI particles possess pore volumes that may be accessible to solvent molecules. If solvent molecules are small enough to penetrate into the available pores, then some solvent is lost from the suspending polymer solution thereby increasing the polymer concentration. As an additional consequence, the reduced volume of the suspending medium effectively increases the zeolite volume fraction in the suspension. These two concentration changes contribute to a rise in viscosity. Thus, it is imperative to derive model equations for the effective concentrations of the polymer and zeolite.

Models for effective polymer concentration and effective zeolite volume fraction

We define a dimensionless fractional absorption parameter, α, as the weight of absorbed solvent (NMP) per unit mass of dry zeolite in suspension. We denote the densities of polymer solution, solvent, zeolite particles, and overall suspension as ρ_{psol}, ρ_{solv}, ρ_z and ρ_{susp}, respectively. The weight fraction of zeolite in the suspension is w_z, and the as-prepared nominal weight fraction of polymer in the suspending medium is w_p. As a result of solvent absorption, the Ultem (polymer) weight fraction in the continuous phase deviates from the nominal values and must be corrected to $w_{p,eff}$. Similarly, although w_z remains constant, the rheologically more relevant volume fraction of zeolite in the suspension also must be corrected for absorption effects, $\varphi_{z,eff}$. Using this nomenclature, the absorption-corrected polymer weight fraction in the suspending medium and effective zeolite volume fraction are derived below.

Using a basis of 1-g zeolite suspension, we define the following:

fractional absorption parameter,

$$\alpha = \frac{\text{weight of absorbed solvent}}{\text{weight of dry zeolite}}$$

weight fraction of suspending medium in suspension, $1 - w_z$
weight fraction of polymer in suspending medium (before absorption), w_p
weight fraction of polymer in suspension, $w_p\ (1 - w_z)$
weight fraction of solvent in suspension, $(1 - w_z)(1 - w_p)$

After solvent absorption, we have as follows:

weight of solvent absorbed in zeolite particles, $\alpha \cdot w_z$
weight of solvent left in suspending medium, $(1 - w_p)\ (1 - w_z) - \alpha \cdot w_z$
effective polymer weight fraction in suspending medium,

$$w_{p,eff} = \frac{w_p(1-w_z)}{w_p(1-w_z) + (1-w_p)(1-w_z) - \alpha w_z}.$$

$$w_{p,eff} = \frac{w_p(1-w_z)}{(1-w_z) - \alpha w_z} \tag{2}$$

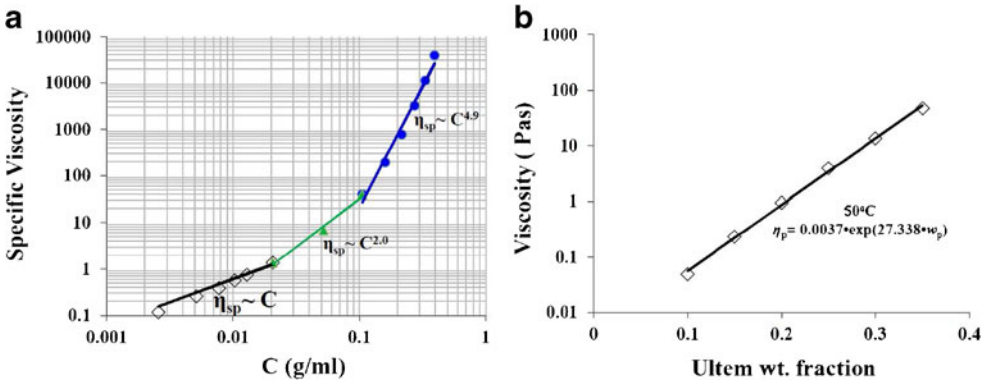

Fig. 3 **a** Specific viscosity as a function of Ultem concentration showing the dilute, semidilute unentangled, and semidilute entangled concentration regimes at 50 °C. **b** Viscosity of Ultem/NMP solutions versus polymer concentration with an exponential fit to data at 50 °C

The absorption-corrected effective zeolite volume fraction is derived below.

volume of absorbed solvent, $\frac{\alpha \cdot w_z}{\rho_{solv}}$

volume of particles, $\frac{w_z}{\rho_z}$

volume of suspension before solvent absorption, $\frac{1}{\rho_{susp}}$

effective zeolite volume fraction,

$$\varphi_{z,eff} = \frac{\left(\frac{w_z}{\rho_z}\right)}{\left(\frac{1}{\rho_{susp}}\right) - \left(\frac{\alpha \cdot w_z}{\rho_{solv}}\right)}.$$

$$\varphi_{z,eff} = \frac{w_z}{\frac{\rho_z}{\rho_{susp}} - \alpha w_z \frac{\rho_z}{\rho_{solv}}} \tag{3a}$$

The overall suspension density, which also depends on solvent absorption, can be expressed in terms of other variables as follows:

$$\rho_{susp} = \frac{1}{[\text{vol. of polymer soln}]+[\text{vol. of zeolite in soln}]-[\text{vol. of absorbed solvent}]}$$

$$\frac{\rho_z}{\rho_{susp}} = w_z + (1 - w_z)\frac{\rho_z}{\rho_{psol}} - \alpha w_z \frac{\rho_z}{\rho_{solv}} \tag{3b}$$

Combining Eqs. 3a and 3b leads to the expression for effective zeolite volume fraction in Eq. 3c:

$$\varphi_{z,eff} = \frac{w_z}{w_z + (1 - w_z)\frac{\rho_z}{\rho_{psol}} - 2\alpha w_z \frac{\rho_z}{\rho_{solv}}} \tag{3c}$$

As expected, the equations for absorption-corrected concentrations show that the concentration of polymer in the suspending phase and the zeolite particle loading both increase for increased solvent absorption.

Models for effective viscosities

From the measured viscosity flow curves of different concentrations of Ultem/NMP solutions, a correlation for viscosity as a function polymer weight fraction at 50 °C is determined as follows:

$$\eta_p = 0.0037 \cdot e^{27.3 \cdot w_p} (\text{Pa s}) \tag{4}$$

Hence, using Eq. 2, the corrected effective viscosity of polymer solution after solvent absorption becomes

$$\eta_{p,eff} = 0.0037 \cdot e^{27.3 \cdot w_{p,eff}} = 0.0037 \cdot e^{\left[27.3 \cdot \frac{w_p(1-w_z)}{(1-w_z)-\alpha w_z}\right]} \tag{5}$$

This equation can be expressed in a form that shows the relative increase in the viscosity of polymer solution as result of solvent absorption:

$$\frac{\eta_{p,eff}}{\eta_p} = e^{\left[27.3 \cdot \frac{\alpha w_p w_z}{(1-w_z)-\alpha w_z}\right]} \tag{6}$$

The Krieger–Dougherty (KD) model (Krieger and Dougherty 1959) for suspension viscosity is frequently used for viscosity predictions of hard sphere suspensions, using the intrinsic viscosity, $[\eta]$, and maximum packing fraction, φ_m, as key parameters. There are several other models for predicting suspension viscosity; many of these models, however, only give good predictions for particular ranges of particle concentrations. Therefore, we have chosen to use the KD model for our suspension viscosity because of its versatile application to a wide range of particle concentrations and the convenient physical interpretation of its input parameters:

$$\eta_r = \left(1 - \frac{\varphi}{\varphi_m}\right)^{-[\eta]\varphi_m} \tag{7}$$

Inserting the absorption-corrected zeolite concentration (Eq. 3c) into the Krieger–Dougherty model yields the equation below; η_{susp} and $\eta_{p,eff}$ are, respectively, the measured suspension viscosity and the effective viscosity of the suspending medium, i.e. the polymer solution:

$$\eta_{r,eff} = \frac{\eta_{susp}}{\eta_{p,eff}} = \left[1 - \frac{w_z}{\varphi_m\left(w_z + (1 - w_z)\frac{\rho_z}{\rho_{psol}} - 2\alpha\varphi_z\frac{\rho_z}{\rho_{solv}}\right)}\right]^{-[\eta]\varphi_m} \tag{8}$$

It should be noted that in experiments, the suspension viscosity is naturally compared to the viscosity of the original polymer solution, which gives rise to an apparent relative viscosity, $\eta_{r,app}$:

$$\eta_{r,app} = \frac{\eta_{susp}}{\eta_p} = \frac{\eta_{p,eff}}{\eta_p}\left[1 - \frac{w_z}{\varphi_m\left(w_z + (1 - w_z)\frac{\rho_z}{\rho_{psol}} - 2\alpha\varphi_z\frac{\rho_z}{\rho_{solv}}\right)}\right]^{-[\eta]\varphi_m} \tag{9a}$$

$$\eta_{r,app} = e^{\left(27.3\frac{\alpha w_p w_z}{(1-w_z)-\alpha w_z}\right)} \times \left[1 - \frac{w_z}{\varphi_m\left(w_z + (1 - w_z)\frac{\rho_z}{\rho_{psol}} - 2\alpha\varphi_z\frac{\rho_z}{\rho_{solv}}\right)}\right]^{-[\eta]\varphi_m} \tag{9b}$$

Using Eq. 9b and assuming that porous particles behave as hard spheres, the effect of solvent absorptions on the viscosity of suspensions of porous particles in a polymer solution can be calculated. The variation of the apparent relative viscosity as a function of particle volume fraction at different values of the absorption parameter α is plotted and presented in Fig. 4. The plot assumed a starting suspending medium of a 30 wt% Ultem/NMP at 50 °C and that MFI particles behaved as model hard spheres with $[\eta] = 2.5$ and $\varphi_m = 0.63$. The graph shows clearly that the apparent relative viscosity increases strongly with the amount of solvent absorbed. The effect is more important at high particle loadings, because higher loadings result in more solvent absorption from the suspending medium; as

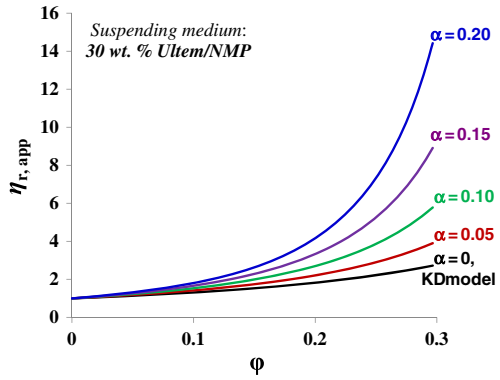

Fig. 4 The apparent relative viscosity of suspensions of MFI particles in a 30 wt% Ultem/NMP solution for different values of the absorption parameter α

a consequence, an exponential increase in the viscosity of the polymer solution according to Eq. 6 is realized. The variation of the apparent relative viscosity as a function of polymer concentration at a fixed particle concentration (35 wt% MFI zeolite) is shown in Fig. 5 for the same values of α; again, the polymer is assumed to be Ultem dissolved in NMP at 50 °C. This graph highlights the fact that the apparent relative viscosity is even most enhanced by solvent absorption at higher polymer concentrations. This treatment does not take into account the effect of electroviscous effects, particle geometry or viscoelastic matrices on MFI suspension viscosity since these nonidealities are independent of solvent absorption. In light of these results, it is important to determine the value of α as accurately as possible for the suspensions of porous particles. In the next section, a method for the experimental determination of α from rheological measurements will be described.

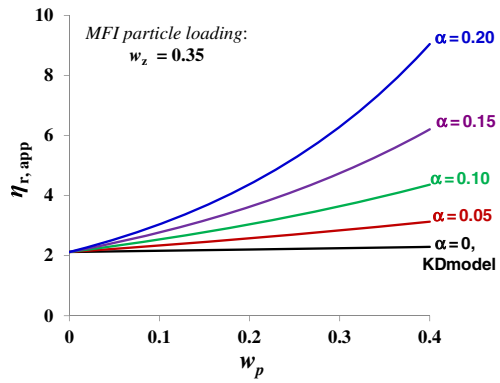

Fig. 5 The apparent relative viscosity of suspensions with 35 wt% MFI particles in suspending Ultem/NMP media with varying nominal weight fractions of polymer for different values of the absorption parameter α

Results and discussions

Figure 6 shows experimental data on the apparent relative viscosities of calcined (porous) 130-nm USZ-MFI suspensions in 30 wt% Ultem/NMP solutions as a function of the apparent particle volume fraction, φ_z. This is only an apparent volume fraction because it is calculated based on the density of dry, calcined MFI particles. In reality, the effective volume fraction is greater than the apparent volume fraction due to solvent absorption resulting in a decreased volume of the suspending medium. For comparison, the Krieger–Dougherty (Krieger and Dougherty 1959) hard sphere model prediction (with $[\eta] = 2.5$ and $\varphi_m = 0.63$) is shown in the same figure. It is clear from this graph that there is a significant disparity between the data and the model prediction.

We propose three reasons for this discrepancy. The first and major cause of deviations from hard sphere behavior is the effect described in the previous section: absorption of NMP solvent molecules from the polymer solution into the MFI zeolite pores. The apparent volume fraction of the zeolite suspension as plotted on the horizontal axis of Fig. 5 is therefore not an accurate depiction of the effective particle volume fractions expressed in Eqs. 3a and 3c, but without knowing α, the effective volume fraction cannot be calculated. The apparent relative viscosity in Fig. 5, calculated as the measured suspension viscosity divided by a 30 wt% Ultem/NMP solution viscosity, is a combination of increased particle contribution to viscosity plus an additional contribution to the viscosity from the increased polymer concentration above the assumed nominal 30 wt% Ultem in NMP. The effect is captured in Eq. 9a, b, provided that the particles behave as hard spheres and that slight variations in the suspending medium composition do not affect the particle contribution to the suspension viscosity. A secondary cause for the deviations in Fig. 6 could be that the MFI zeolite particles acquires surface charge in

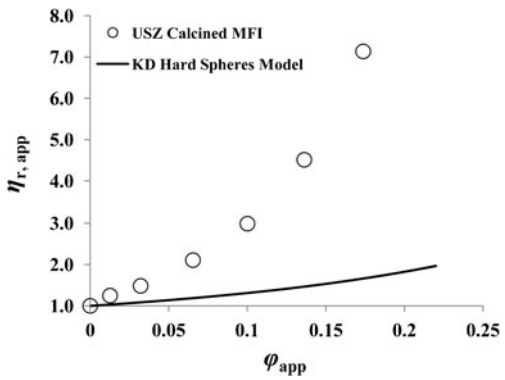

Fig. 6 Relative viscosity as a function of particle volume fraction; large deviation between calcined MFI suspension and the Krieger–Dougherty hard sphere model prediction is observed

solution, consequently showing electroviscous effects and thus deviating from the model of hard sphere prediction of the Krieger–Dougherty equation. Thirdly, the fact that the particles are suspended in viscoelastic polymer solution may also contribute to deviation from hard sphere predictions. Although it is known that such nonidealities exist, it is generally not known a priori how strongly these affect the suspension viscosity. We therefore devised a strategy to experimentally determine the absorption parameter α without having to make assumptions about the applicability of the Krieger–Dougherty equation.

Figure 7 presents the experimental data that were used to determine the solvent absorption parameter α for MFI particles. In this approach, a direct comparison of the viscosity of suspensions of comparable concentrations of uncalcined and calcined ST MFI particles in Ultem/NMP solutions were used to estimate the solvent absorption parameter.

As expected, in all cases, the viscosity of the calcined (porous) zeolite suspensions is greater than the corresponding uncalcined zeolite suspensions due to the absorption of solvent in the suspensions of calcined MFI particles.

In Fig. 8, the apparent relative viscosity in the zero shear limit is plotted versus the apparent particle volume fraction for the uncalcined MFI suspensions, which are nonporous and calcined MFI suspensions. This uncalcined MFI suspension data was used to determine empirical fit parameters, β and γ, needed to account for deviations from the Einstein (1911) and Batchelor (1977) coefficients arising from hard sphere model assumptions such as particle nonsphericity and electroviscous effects. The semiempirical relationship between the relative viscosity and particle volume fraction

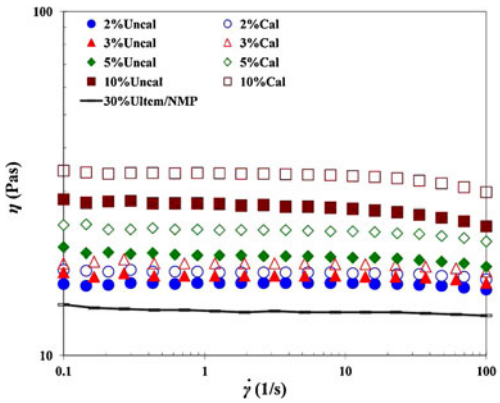

Fig. 7 Flow curves for polymer solution and suspensions of uncalcined and calcined MFI particles. *Unfilled* and *filled symbols* represent porous and nonporous MFI particles, respectively, while the different *geometric symbols* indicate MFI concentration: *circle* (2 wt% MFI), *triangle* (3 wt% MFI), *diamond* (5 wt% MFI), *square* (10 wt% MFI)

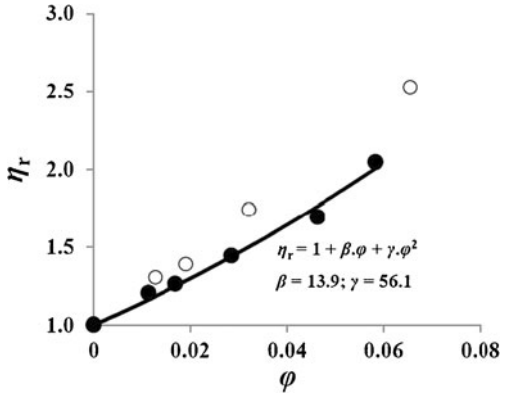

Fig. 8 A quadratic fit to the relative viscosity versus volume fraction of uncalcined ST MFI particle suspension to determine the intrinsic viscosity, β, and the interaction term coefficient, γ, for MFI particles. *filled circle*, uncalcined MFI; *unfilled circle*, calcined MFI

for the uncalcined MFI particle suspension from Fig. 8 is given by the following:

$$\eta_r = 1 + \beta.\varphi + \gamma.\varphi^2 \tag{10}$$

A second-order polynomial dependence of relative viscosity on particle volume fraction is used to fit our data for uncalcined MFI suspensions in this range of dilute to semidilute concentration of particles. Analysis was carried out in this regime so that the important physical attributes of a suspension (i.e., the intrinsic viscosity and the effective collision diameter) are in play, while maintaining a sufficiently low particle concentration to facilitate mathematical analysis for absorption parameter.

From the data in Fig. 8, the intrinsic viscosity of uncalcined ST MFI particles was found to be roughly 13.9, much greater than the intrinsic viscosity of 2.5 for the model of hard sphere suspensions. There are a number factors contributing to the observed deviation: (1) the aspect ratio of the MFI particles is not unity and (2) electroviscous effects due to charging of MFI particle surfaces in the solution. Together, these effects conspire to significantly increase the intrinsic viscosity of uncalcined MFI in a polymer solution. Similarly, the coefficient of the second-order interaction term is 56.1, which is much greater than the Batchelor prediction of 6.2 for hard spheres. This deviation may be largely due to secondary electroviscous effects (Russel 1976) since the MFI particle acquires an electric double layer in solution.

For the uncalcined MFI suspensions, there is no loss of solvent due to absorption, since the pores of the MFI particles are still occupied by the organic templates. Therefore, it is reasonable to expect that the empirical fit obtained for uncalcined MFI particles in Fig. 8 should also correctly capture the relationship between relative viscosity and particle

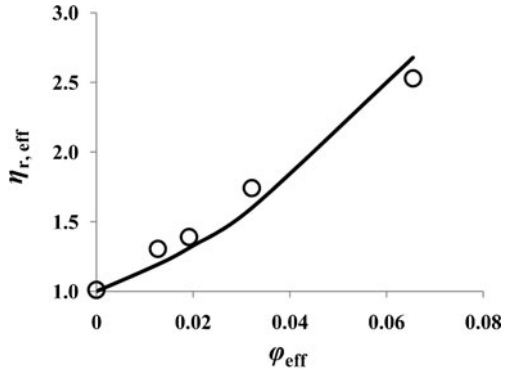

Fig. 9 Effective relative viscosity versus effective volume fraction for calcined MFI particle suspensions (volume fraction corrected with $\alpha = 0.18$); *line* represents model predictions using $\alpha = 0.18$. Effective relative viscosity only accounts for the effect of solvent absorption to suspension viscosity

volume fraction for calcined MFI particle suspensions, provided that the correct effective volume fraction of calcined MFI particles in Eq. 3c is used. For the calcined MFI particle suspension, the effective relative viscosity can then be expressed as follows:

$$\eta_{r,eff} = \frac{\eta_{r,app}}{\exp\left(27.338\frac{w_u w_z \alpha}{1-(1-\alpha)w_z}\right)} = 1 + 13.9\varphi_{z,eff} + 56.1\varphi_{z,eff}^2 \quad (11)$$

Using the expression for $\varphi_{z,eff}$ in Eq. 3c, Eq. 11 can be solved for α using $\langle \eta_{r,app} \rangle$ and $\langle w_z \rangle$ as input vectors that contain the data from the measurements on porous, calcined MFI suspensions. Using a suitable optimization scheme, the solvent absorption parameter was determined as 0.18. This value is in good agreement with the theoretical pore volume of MFI particles of 0.175 calculated based on information in the reference (Flanigen et al. 1978). Figure 9 compares the experimental data of calcined MFI with the model predictions after incorporating the determined absorption parameter value, $\alpha = 0.18$ in Eqs. 3c and 11 to correct for solvent absorption. As expected, the experimental result and simulation result show a good agreement.

Conclusions

We have shown that when solvent molecules are of comparable size to the pore volume windows of porous zeolite particles, the rheology of suspensions of such particles in polymer solutions can be drastically altered by solvent absorption. Absorption of solvent from the suspending medium into porous zeolite particles increases the concentrations of the polymer in the continuous phase and the concentration of dispersed particles. Consequently, such suspensions can have viscosities that significantly exceed model predictions based on nonporous particles. Corrections for these deviations can be achieved by taking into account the changes in polymer and particle concentrations. We present simple models that use a solvent absorption parameter, α, defined as the weight of solvent absorbed per gram of porous zeolite particle to make the necessary corrections. We developed and validated an experimental rheological technique to determine α. The value $\alpha = 0.18$ that was found for MFI zeolites was found to be in good agreement with the theoretical pore volume available within MFI particles based on the crystal structure. Based on these findings, a model can be proposed to correctly predict the effect of absorption on the viscosity of suspensions of porous particles.

Acknowledgments We are grateful to the ExxonMobil Corporation for the financial support for this work. We also wish to express our gratitude to Professors Bill Koros and Chris Jones for numerous discussions on this work.

References

Batchelor GK (1977) Effect of Brownian-motion on bulk stress in a suspension of spherical-particles. J Fluid Mech 83:97–117

Booth F (1950) The electroviscous effect for suspensions of solid spherical particles. Proc R Soc Lond Ser A-Math Phys Sci 203:533–551

Cheng CH, Bae TH, McCool BA, Chance RR, Nair S, Jones CW (2008) Functionalization of the internal surface of pure-silica MFI zeolite with aliphatic alcohols. J Phys Chem C 112:3543–3551

Chung TS, Jiang LY, Li Y, Kulprathipanja S (2007) Mixed matrix membranes (MMMs) comprising organic polymers with dispersed inorganic fillers for gas separation. Prog Polym Sci 32:483–507

de Oliveira IS, van den Noort A, Padding JT, den Otter WK, Briels WJ (2011) Alignment of particles in sheared viscoelastic fluids. J Chem Phys 135:104902

Einstein A (1906) A new determination of the molecular dimensions. Ann Phys 19:289–306

Einstein A (1911) A new determination of the molecular dimensions (vol 19, pg 289, 1906). Ann Phys 34:591–592

Ekiner OM, Vassilatos G (1990) Polyaramide hollow fibers for hydrogen methane separation–spinning and properties. J Membr Sci 53:259–273

Ekiner OM, Vassilatos G (2001) Polyaramide hollow fibers for H_2/CH_4 separation–II. Spinning and properties. J Membr Sci 186:71–84

Flanigen EM, Bennett JM, Grose RW, Cohen JP, Patton RL, Kirchner RM, Smith JV (1978) Silicalite, a new hydrophobic crystalline silica molecular-sieve. Nature 271:512–516

Fyfe CA, Gobbi GC, Klinowski J, Thomas JM, Ramdas S (1982) Resolving crystallographically distinct tetrahedral sites in silicalite and ZSM-5 by solid-state NMR. Nature 296:530–533

Husain S (2006) Mixed matrix dual layer hollow fiber membranes for natural gas separation. PhD Dissertation, Georgia Institute of Technology, Atlanta

Husain S, Koros WJ (2007) Mixed matrix hollow fiber membranes made with modified HSSZ-13 zeolite in polyetherimide polymer matrix for gas separation. J Membr Sci 288:195–207

Jeffery GB (1922a) The motion of ellipsoidal particles in a viscous fluid. Proc Roy Soc (London), Ser A-Containing Papers Mathematical Physical Character 102:161–179

Jeffery GB (1922b) The rotation of two circular cylinders in a viscous fluid. Proc Roy Soc (London), Ser A-Containing Papers Mathematical Physical Character 101:169–174

Kitano T, Kataoka T, Shirota T (1981) An empirical equation of the relative viscosity of polymer melts filled with various inorganic fillers. Rheol Acta 20:207–209

Krieger IM, Dougherty TJ (1959) A mechanism for non-Newtonian flow in suspensions of rigid spheres. Trans Soc Rheol 3:137–152

Mahajan R, Koros WJ (2000) Factors controlling successful formation of mixed-matrix gas separation materials. Ind Eng Chem Res 39:2692–2696

Mahajan R, Koros WJ (2002a) Mixed matrix membrane materials with glassy polymers. Part 1. Polym Eng Sci 42:1420–1431

Mahajan R, Koros WJ (2002b) Mixed matrix membrane materials with glassy polymers. Part 2. Polym Eng Sci 42:1432–1441

Malkin AY (2012) Non-Newtonian viscosity in steady-state shear flows. J Non-Newtonian Fluid Mech 192:48–65

Metzner AB (1985) Rheology of suspensions in polymeric liquids. J Rheol 29:739–775

Moore TT, Mahajan R, Vu DQ, Koros WJ (2004) Hybrid membrane materials comprising organic polymers with rigid dispersed phases. AIChE J 50:311–321

Mueller S, Llewellin EW, Mader HM (2010) The rheology of suspensions of solid particles. Proc R Soc A-Math Phys Eng Sci 466:1201–1228

Pabst W, Gregorova E, Berthold C (2006) Particle shape and suspension rheology of short-fiber systems. J Eur Ceram Soc 26:149–160

Pasquino R, Grizzuti N, Maffettone PL, Greco F (2008) Rheology of dilute and semidilute noncolloidal hard sphere suspensions. J Rheol 52:1369

Pasquino R, Panariello D, Grizzuti N (2012) Migration and alignment of spherical particles in sheared viscoelastic suspensions. A quantitative determination of the flow-induced self-assembly kinetics. J Colloid Interface Sci 394:49–54

Paul DR, Kemp DR (1973) Diffusion time lag in polymer membranes containing adsorptive fillers. J Polym Sci Part C-Polym Symp 41:79–93

Robeson LM (1991) Correlation of separation factor versus permeability for polymeric membranes. J Membr Sci 62:165–185

Robeson LM (2008) The upper bound revisited. J Membr Sci 320:390–400

Russel WB (1976) Low-shear limit of secondary electroviscous effect. J Colloid Interface Sci 55:590–604

Schoeman BJ (1997a) A spectroscopic study of the initial stage in the crystallization of TPA-silicalite-1 from clear solutions. In: Chon H, Ihm SK, Uh YS (eds) Progress in zeolite and microporous materials, Pts a-C, vol 105, pp 647–654

Schoeman BJ (1997b) The homogeneous nature of clear TPA-silicalite-1 precursor solutions. Microporous Mater 9:267–271

Snijkers F, Pasquino R, Vermant J (2013) Hydrodynamic interactions between two equal-sized spheres in viscoelastic fluids in shear flow. Langmuir 29:5701–5713

Stimson M, Jeffery GB (1926) The motion of two spheres in a viscous fluid. Proc Roy Soc (London), Ser A-Containing Papers Mathematical Physical Character 111:110–116

Vaynberg KA, Wagner NJ (2001) Rheology of polyampholyte (gelatin)-stabilized colloidal dispersions: the tertiary electroviscous effect. J Rheol 45:451–466

Wallace DW, Staudt-Bickel C, Koros WJ (2006) Efficient development of effective hollow fiber membranes for gas separations from novel polymers. J Membr Sci 278:92–104

Watterson IG, White LR (1981) Primary electroviscous effect in suspensions of charged spherical-particles. J Chem Soc-Faraday Trans Ii 77:1115–1128

Zhou Z, Solomon MJ, Scales PJ, Boger DV (1999) The yield stress of concentrated flocculated suspensions of size distributed particles. J Rheol 43:651

Zurita L, Carrique F, Delgado AV (1994) The primary electroviscous effect in silica suspensions - ionic-strength and ph effects. Colloids Surf A-Physicochem Eng Aspects 92:23–28